Int J Intell Robot Appl (2017) 1:195–208
DOI 10.1007/s41315-017-0019-5

REGULAR PAPER

2D maneuverable robotic fish propelled by multiple ionic polymer–metal composite artificial fins

Zhihang Ye[1] · Piqi Hou[1] · Zheng Chen[1] · IEEE Member

Received: 17 November 2016 / Accepted: 5 April 2017 / Published online: 13 April 2017

Abstract Bio-inspired robotic fish are proving to be promising underwater vehicles whose high propulsion efficiency, stealth, and compact size make them suitable for remote sensing missions in intelligence collection, environmental monitoring, and fishing agriculture. In this research, a two-dimensional (2D), maneuverable, bio-inspired robotic fish propelled by multiple ionic polymer-metal composite artificial fins was developed. The movement of this fish, equipped with one caudal fin and two pectoral fins, was then modeled by a nonlinear dynamic model for design and control purposes. Experiments were conducted to verify the model's capabilities of characterizing the robotic fish's 2D movement. The forward-swimming speed reached about 12 mm/s and the turning speed reached about 2.5 deg/s.

Keywords Robotic fish · Ionic polymer-metal composite · Dynamic modeling

1 Introduction

A mobile underwater sensing network (MUSN) is one of the key technologies in environmental monitoring, aquaculture, and marine life studies (Ryuh et al. 2015; Wang et al. 2014). For example, Porifiri's group employed robotic fish to study the behavior of zebrafish (Bartolini et al. 2016; Kopman et al. 2015; Mwaffo et al. 2017; Ruberto et al. 2016; Zienkiewicz et al. 2015). In these types of applications, robotic fish with two-dimensional (2D) and stealthy underwater maneuvering capabilities are needed to build a viable MUSN system. In recent years, more and more researchers and companies have become attracted to this area of biomimetic underwater robot research, including robotic fish (Guo et al. 2003; Hu et al. 2006; Kim et al. 2005; Lauder et al. 2007; Morgansen et al. 2007; Tan et al. 2006; y Alvarado and Youcef-Toumi 2006; Zhou and Low 2012), robotic jelly fish (Najem et al. 2012; Villanueva et al. 2011; Yeom and Oh 2009), and robotic rays (Chen et al. 2011a, 2012; Gao et al. 2007; Wang et al. 2009). For example, the Festo and Evologics companies have developed bionic robotic manta rays using fluid muscles (Evologics 2009; Festo 2008). Most of this research work is based on a traditional motor-driven mechanism to simulate the aquatic animals' flapping actions. As a result, power transmission is needed to convert the motors' rotation motion into a flapping motion. Hence, in addition to bulky electric motors, this mechanism still requires additional space for the power transmission devices, which will also lower the energy efficiency and render it unsuitable for space-limited bio-inspired robots. The gear set and levers in these transmission devices also cause unwanted noise, which makes the robot unfriendly to marine animals and more detectable. Biological fish muscles can generate compliant actuation in order to achieve high-energy, efficient, and stealthy underwater propulsion, which is difficult for traditional motors and power transmission systems (Lauder et al. 2011). Smart materials can satisfy these requirements because they are light weight, flexible, and capable of directly generating a large flapping motion. These desirable features make them promising in building energy-efficient, 2D-maneuverable, stealthy, and compact underwater bio-inspired robots (Lauder et al. 2011).

Among the variety of smart materials, electroactive polymers (EAPs) can generate a large deformation with electrical stimuli (Bar-Cohen 2000). EAPs are often

✉ Zheng Chen
zheng.chen@wichita.edu

[1] Department of Electrical Engineering and Computer Science, Wichita State University, Wichita, KS 67260-0083, USA

referred to as artificial muscles because of their muscle-like actuation. Based on their working configurations, they are divided into two categories: dielectric EAPs and ionic EAPs. Dielectric EAPs are capable of generating a large force and large deformation (Carpi et al. 2011; Pelrine et al. 2000; Suo 2010) under high actuation voltage (typically higher than 1 kV), which limits their applications in a water-contact environment. On the other hand, ionic polymer-metal composites (IPMCs) are more suitable and even necessary for use in a water environment. An IPMC actuator consists of an ion exchange membrane coated with two metal electrodes (Shahinpoor and Kim 2001), such as gold or platinum. When a small voltage (less than 2 V) is applied on the IPMC, the electric potential causes ion transportation from the anode side to the cathode side, which leads to a swelling effect on the cathode side and a shrinking effect on the anode side. As a result, the IPMC bends to the anode side, which results in a flapping actuation movement. Figure 1 shows the actuation mechanism of an IPMC. Considering the fact that they are soft, lightweight, low power consuming, and capable of generating a flapping motion, IPMCs are ideal for their use as actuators of compact underwater bio-inspired robots.

Many researchers have devoted their efforts toward IPMC-powered underwater robots (Guo et al. 2003; Hu et al. 2006; Kim et al. 2005; Tan et al. 2006). Tan et al. developed an IPMC caudal fin propelled robotic fish (Tan et al. 2006), and Chen et al. developed a corresponding speed model for the control of the robotic fish (Chen et al. 2010). Robotic manta rays and cow-nose rays have also been developed with IPMC-driven structures (Chen et al. 2011b, 2012; Punning et al. 2004). Steady turning motion under periodic but asymmetric actuation of the IPMC can be accomplished (Chen et al. 2010; Aureli et al. 2010; Ye et al. 2007). However, since IPMCs working in a robotic fish have limited bending range due to the requirements of size and activating frequency, a robotic fish with a single caudal fin has very limited maneuverability for 2D or 3D swimming. Hence, inspired by biological fish, a multiple-fin propulsion and maneuvering system is needed to achieve a better 2D or 3D maneuvering capability.

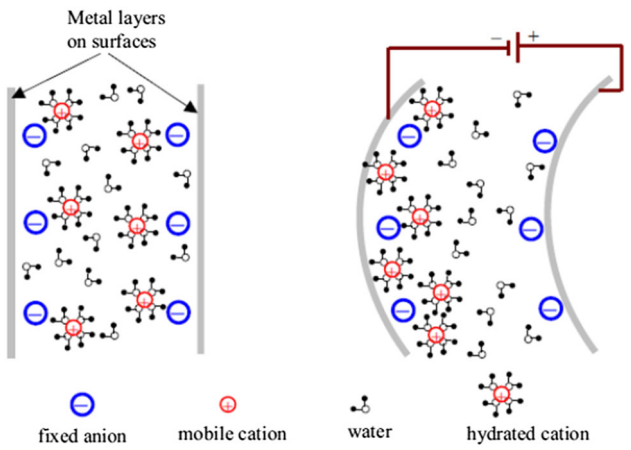

Fig. 1 Actuation mechanism of IPMC (Chen and Tan 2008)

For control design purposes, a dynamic model is needed to describe the behavior of robotic fish and their interaction with the environment. Many existing research studies have been done on this topic (Kopman et al. 2015; Guo 2006; Shao et al. 2008; Wang et al. 2015; Wang and Tan 2013; Yu et al. 2004). Several fish species use their pectoral fins primarily for propulsion and as a stabilizing method within their living environment (Walker 2004), but the pectoral fin is also necessary for maneuverability (Behbahani et al. 2013; Hu 2009). Behbahani et al. (2013) derived a model for a robotic fish with two pectoral fins, using the blade element theory to evaluate the hydrodynamic forces applied on the fish's body. Hu (2009) researched the pectoral fin rowing propulsion model based on the drag mechanism.

This paper presents a 2D maneuverable and wireless controlled robotic fish that is fully actuated by IPMC artificial muscles. Inspired by biological fish, the artificial fish is capable of generating forward and steering movements with its caudal and pectoral fins. Each fin consists of an IPMC actuator in order to provide an energy-efficient and compliant movement. With the help of IPMCs, a complex power transmission device is not needed, and the fish can use multiple-fin propulsion to achieve 2D stealthy movement in a compact space while the actuation noises are largely diminished. An on-board controller and photon wireless communication module powered by a lithium battery are assembled for the robotic fish to enable its 2D swimming and wireless controllable capabilities. A dynamic model that describes the 2D dynamic movement of fish is also developed for design and control purposes. The thrust force produced by each actuator is evaluated by incorporating Lighthill's theory of elongated-body propulsion (Chen et al. 2010) and IPMC actuation dynamics (Chen and Tan 2008). The final model then incorporates all forces of the IPMC fins into a 2D body dynamic model (Wang and Tan 2013). Experiments were conducted to evaluate the accuracy of the obtained dynamic model. Since the robotic fish that is propelled by IPMC artificial muscle fins can swim quietly, aquatic animal behavior studies will be one of the future applications of this type of robotic fish.

The rest of this paper is organized as follows: Design of the robotic fish is shown in Sect. 2. Development of the dynamic model of the robotic fish is presented in Sect. 3. The steps of fish fabrication are outlined in Sect. 4. Experimental results are discussed in Sect. 5. Conclusions and future work are presented in Sect. 6.

2 Design of 2D maneuverable robotic fish

A mobile underwater sensing network requires agents with 2D or 3D mobility, which in recent years is still underdeveloped. The highly adept maneuverability of biological fish is achieved by their multiple cooperative fins. Inspired by this, the robotic fish proposed in this paper uses three fins: one caudal fin for propulsion and two pectoral fins for steering, as shown in Fig. 2. The robotic fish is designed to perform 2D on the surface of water. The caudal fin is horizontal to the water surface. Some aquatic animals, such as whales and sea lions, use vertical motion on caudal fin to generate thrust. In this paper, we want to test the swimming performance of the robotic fish with vertical motion on the caudal fin. Future work will be focused on investigating the difference between the vertical and horizontal motions on the caudal fin. The main reason that we design the passive fin to mimick the caudal fin of a tuna fish is to improve the thrust force. Based on the Lighthill theory, the thrust force increases as the width at the end of fin increases but the loading effect also increases. To reduce the loading effect, the surface area needs to be small. We found that tuna caudal fin can meet both requirements: enlarged ending width and small surface area. This paper is the first to demonstrate the 2D maneuverable robotic fish with IPMC-powered fins.

2.1 2D maneuvering mechanism

The 2D maneuvering capability of robotic fish can be achieved by using different combinations of activated fins. Figure 3 shows the control method to realize 2D movement of the robotic fish, where the center of mass is located at point G. All three fins are activated to generate thrust for forward swimming—the caudal fin is in charge of the main thrust, and the two pectoral fins contribute to auxiliary thrust (Chen et al. 2009). When the left pectoral fin and the caudal fin are activated, a thrust for forward swimming is generated, while a steering force is also provided by the left pectoral fin. Because the center of mass is located in the front of the fish body, the force generated by the left pectoral fin will cause a counterclockwise steering moment, which makes the fish turn left. Similarly, when a right turn is needed, the caudal fin and right pectoral fin are activated to obtain a clockwise moment, thus causing the fish to turn right.

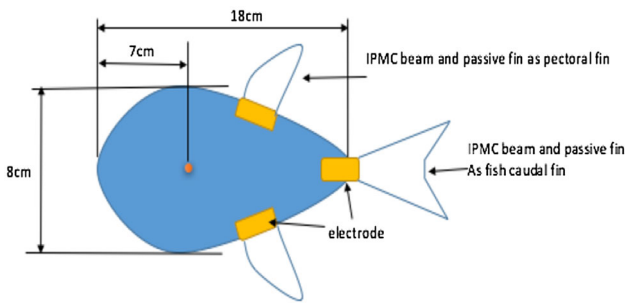

Fig. 2 Design of robotic fish propelled by multi-IPMC fins (*top view*)

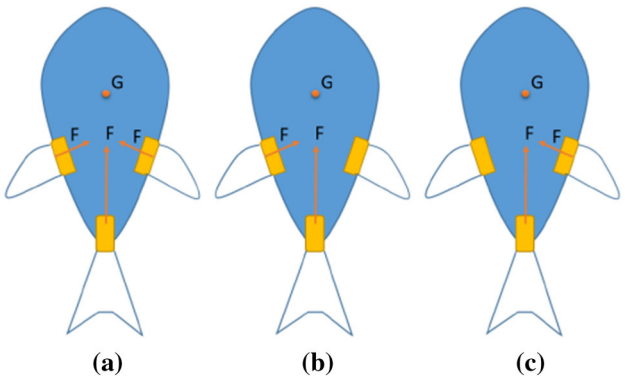

Fig. 3 2D maneuvering capabilities enabled by multiple fish fins: **a** forward swimming; **b** left turn; **c** right turn

2.2 Design of caudal and pectoral fins

Chen et al. (2010), who developed a control-oriented model for robotic fish propelled by an IPMC caudal fin, found that attaching a passive fin to the IPMC beam can strengthen the generated force. Based on the Lighthill theory, the thrust generated by a fish fin is proportional to the square of the width at the fin, that is, the wider the end of the fin, the larger the generated thrust. However, if the entire fin is composed of IPMC, then the large area causes a high capacitance of IPMC, which will take a longer time to charge, thus slowing down its response time. To achieve a high flapping frequency and large width at the end of the fin, a passive element is attached to the IPMC artificial muscle. In this paper, a similar structure of a hybrid caudal fin is used, as shown in Fig. 4a, as well as a triangle-shaped pectoral fin, as shown in Fig. 4b. Each fin consists of only one rectangular IPMC beam attached to a passive fin. The shapes of the fins mimic that of a tuna fish. The main reason for designing the passive fin to mimic the caudal fin of a tuna fish is to improve the thrust force. Based on the Lighthill theory, the thrust force increases as the width at the end of the fin increases but the loading effect also increases. To reduce the loading effect, the surface area

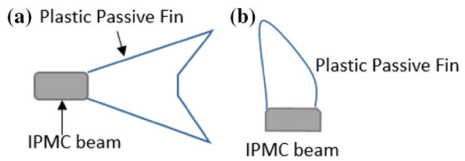

Fig. 4 Design of hybrid fins: **a** caudal fin; **b** pectoral fin

needs to be small. We found that the tuna caudal fin can meet both requirements: enlarged ending width and small surface area.

2.3 Wireless control system design

A wireless communication method is desirable to control the robotic fish remotely in a mobile sensing network. An on-board control system for the robotic fish was developed for controlling functions. All fins have separate control channels and driver units to achieve different combinations of fin activation. The block diagram of this on-board wireless control system design is shown in Fig. 5. A microcontroller (Particle Photon) is used to take orders and generate control signals for the H-bridges of the caudal and pectoral fins.

3 Robotic fish dynamic model

This section presents the model dynamics of the robotic fish in the X–Y plane. The model consists of the thrust dynamics of the threes fins, and the thrusts are incorporated into the dynamic model of the fish body.

3.1 Body dynamics

Since the velocity of robotic fish is quite small in this application, the coupling in the body-fixed coordinate between velocity in the x direction (u), velocity in the y direction (v), and yaw motion (r) is negligible. Therefore, the equation of motion can be simplified as follows (Kodati et al. 2007):

$$\dot{u} = \frac{(m_b - m_y)}{m_x} vr + \frac{f_x}{m_x} \tag{1}$$

$$\dot{v} = \frac{(m_b - m_x)}{m_y} ur + \frac{f_y}{m_y} \tag{2}$$

$$\dot{r} = \frac{\tau_z}{I_z} \tag{3}$$

where f_x and f_y are forces in the x and y directions, respectively; m_x and m_y are the robot's effective masses along the x and y directions, respectively; and I_z is the effective inertia along the Z axis. With the kinematic equations, the dynamics of the fish body in inertial coordination can be shown as follows (Wang et al. 2012):

$$\dot{X} = u\cos\psi - v\sin\psi \tag{4}$$

$$\dot{Y} = v\cos\psi + u\cos\psi \tag{5}$$

$$\dot{\psi} = r \tag{6}$$

where ψ is the heading angle of the fish body, which is defined as the angle between the X axis of inertial coordination and x axis of the body-fixed coordinate system.

3.2 Body-added mass

Based on fluid characteristics, when a body moves in fluid, a portion of the surrounding fluid will also move with the body. This moving fluid will cause an additional mass on the moving body, which is called the mass effect. Here, the mass effect is considered an added component (m_a) to the body mass (m_b). In a similar method, an added inertia is also included. With these concerns, a cylinder-shaped body with radius of R is considered as an approximation of the robot's body (Fig. 6). Therefore, the added mass m_{ay} along the y direction and the added inertia along the z direction can be calculated by using slender-body theory (Barbera 2009):

$$m_{ay} = \pi\rho R^2(x_2 - x_1) \tag{7}$$

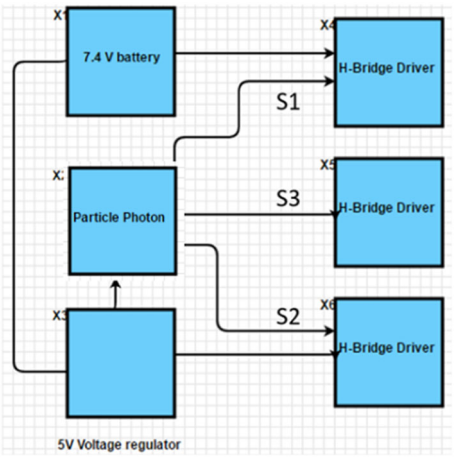

Fig. 5 On-board wireless control system design

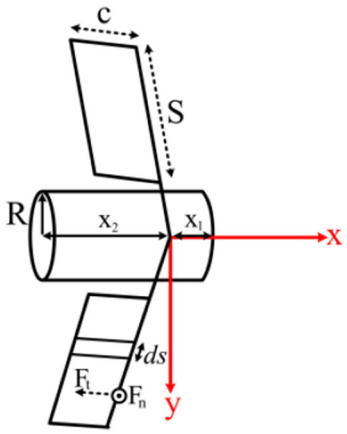

Fig. 6 Robotic fish body component for using slender-body dynamic (Behbahani et al. 2013)

$$I_{az} = \pi\rho R^2 \frac{x_2^3 - x_1^3}{3} \tag{8}$$

where x_1 and x_2 denote the pectoral fins' installing locations, as shown in Fig. 6.

In order to calculate the added mass along the x direction (m_{ax}), the robot body is considered to be an ellipsoid with length of l_e and diameter d_e; then the added mass can be obtained as (Barbera 2009)

$$m_{ax} = \frac{2\pi l_e d_e^2}{6} \tag{9}$$

Finally, the actual mass when the fish is moving in water can be calculated as follows:

$$m_x = m_b + m_{ax} \tag{10}$$

$$m_y = m_b + m_{ay} \tag{11}$$

$$I_z = I_b + I_{az} \tag{12}$$

3.3 Forces and drags

By having the thrust and drag forces in each direction, the total forces along the x and y directions can be easily obtained. As shown previously in Sect. 2, the IPMC thrust can be obtained by considering the fin direction. Figure 7 shows a schematic of the robotic fish body coordination and thrusts generated by IPMC fins in the X–Y plane.

Since the fish is designed to swim in the surface of water, which means it does not change its depth in water, the lift forces in z direction re neglected. As can be seen, to obtain the force along the x and y direction, the synthesis of thrusts generated by fins along each axis is shown below (Behbahani et al. 2013):

$$f_x = T_c + T_r\cos(\theta) + T_l\cos(-\theta) - F_D\cos(\gamma) \tag{13}$$

$$f_y = T_r\sin(\theta) + T_l\sin(-\theta) - F_D\sin(\gamma) \tag{14}$$

$$\tau_z = M_h + M_D \tag{15}$$

where T_c is the caudal actuator's thrust; T_r and T_l are the right and left pectoral fin thrusts, respectively; θ is the angle of the right pectoral fin; $-\theta$ is the angle of the left pectoral fin, since the pectoral fins are symmetrically

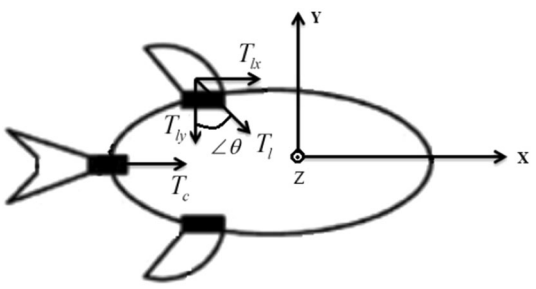

Fig. 7 Robotic fish body coordination in X–Y plane

installed; γ is the angle of attack; and M_h is the total hydrodynamic moment applied to the center of the body (Behbahani et al. 2013):

$$\vec{M}_{hr} = \vec{r}_{Cr} \times \vec{F}_{0r} \tag{16}$$

where $\vec{r}_{Cr}$ is the vector from the center of the body (C) to the base of the right pectoral fin, and $\vec{F}_{0r}$ is the force generated by the right pectoral fin. By following the same process, the left total hydrodynamic moment $\vec{M}_{hl}$, which has the opposite direction of $\vec{M}_{hr}$, can also be obtained. Then the total hydrodynamic moment is calculated as (Behbahani et al. 2013)

$$\vec{M}_h = \vec{M}_{hr} + \vec{M}_{hl} \tag{17}$$

F_D is the drag force, which can be obtained by (Wang and Tan 2013):

$$F_D = \frac{1}{2}\rho|V_c|^2 S_A C_D \tag{18}$$

where S_A is the robotic fish's surface area, C_D is the drag coefficient determined by experiment, and V_c is the linear velocity of robotic fish. M_D is the robotic fish drag moment (Wang and Tan 2013):

$$M_D = -C_M\omega_z^2\mathrm{sgn}(\omega_z) \tag{19}$$

$$\omega_z = \frac{d\gamma(t)}{dt} \tag{20}$$

where ω_z is the angular velocity of the fish body about the z direction, C_M is a coefficient of drag moment that is measured by experiment, and sgn is the sign function.

3.4 IPMC actuator

Applying a small voltage (less than 2 V) to the IPMC will cause a transfer of ions from the anode side to the cathode side, and lead to expansion of the cathode side and shrinkage of the anode side. Chen et al. obtained the average thrust of the IPMC actuator in water using Lighthill's elongated-body theory (Lighthill 1970). Based on this theory, the mean thrust of T produced by the actuator can be calculated by (Chen et al. 2010)

$$\bar{T} = \left[\frac{m}{2}\left(\overline{\left(\frac{\partial w(z,t)}{\partial t}\right)^2} - U^2\overline{\left(\frac{\partial w(z,t)}{\partial z}\right)^2}\right)\right]_{z=L_1} \tag{21}$$

where w is the actuator's bending displacement, U is the fish's velocity on the IPMC's actuation side, $z = L_1$ is the length of the tail, $\overline{(.)}$ denotes the mean value, and m is the

virtual mass density at $z = L_1$, which can be obtained as (Chen et al. 2010)

$$m = \frac{\pi}{4} S_c^2 \rho_w \beta \tag{22}$$

where s_c is the width at the tip of the passive tail, ρ_w is the water density, and β is a non-dimensional parameter that is close to 1. In Eq. (21), $\frac{\partial w(z,t)}{\partial t}$ is the lateral velocity of the IPMC actuator, which can be obtained by calculating the derivative of w with respect to time, and $\frac{\partial w(z,t)}{\partial z}$ is the slope of the IPMC beam at the end of tail ($z = L_1$) (Chen et al. 2010):

$$w(L_1, t) = A_m |H(j\omega)| \sin(\omega t + \angle H(j\omega)) \tag{23}$$

$$\left.\frac{\partial w(z,t)}{\partial z}\right|_{z=L_1} = A_m |H_d(j\omega)| \sin(\omega t + \angle H_d(j\omega)) \tag{24}$$

where A_m and ω are the input sinusoidal voltage's amplitude and frequency, respectively; and $H(j\omega)$ and $H_d(j\omega)$ are the IPMC's transfer functions derived in the work of Chen et al. (2010). Since the IPMC based robotic fish swims at a relative slow speed, compared to the bending motion of IPMC, the base excitation due to the body motion is not considered in the actuation dynamics of IPMC fin. Figure 8 shows a physical illustration of the IPMC beam with a passive fin.

The two transfer functions related to IPMC $H(L_1, s)$ and $H_d(L_1, s)$ are as follows (Chen et al. 2010):

$$H(L_1, s) = H_1(L_0, s) + H_{1d}(L_0, s) \tag{25}$$

$$H_d(L_1, s) = H_{1d}(L_0, s) \tag{26}$$

where

$$H_1(L_1, s) = \frac{(1 + F_s)A_s - B_E E_s}{(1 + C_s)(1 + F_s) - B_s J_s} \tag{27}$$

$$H_{1d}(L_1, s) = \frac{(1 + C_s)E_s - A_s J_s}{(1 + C_s)(1 + F_s) - B_s J_s} \tag{28}$$

in which

$$A_s = \sum_{i=1}^{\infty} \phi_i(L) H_{fi}(s) Q_i(s) \tag{29}$$

$$E_s = \sum_{i=1}^{\infty} \phi_i'(L) H_{fi}(s) Q_i(s) \tag{30}$$

$$D = L_1 - L_0 \tag{31}$$

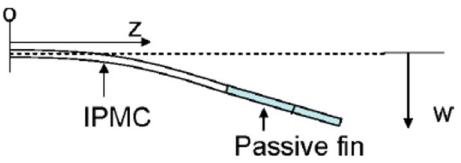

Fig. 8 Physical illustration of IPMC beam with passive fin (Chen et al. 2010)

$$k = \frac{b_1 - b_0}{D} \tag{32}$$

$$M_s \frac{\pi}{4} s^2 \Gamma_2(\omega) \rho_w \tag{33}$$

$$B_s = \sum_{i=1}^{\infty} \frac{\phi_i(L_0) Q_i(s)}{M_i} M_s \begin{bmatrix} \phi_i'(L_0) k_a \\ +\phi_i(L_0) k_b \end{bmatrix} \tag{34}$$

$$C_s = \sum_{i=1}^{\infty} \frac{\phi_i(L_0) Q_i(s)}{M_i} M_s \begin{bmatrix} \phi_i'(L_0) k_b \\ +\phi_i(L_0) k_c \end{bmatrix} \tag{35}$$

$$F_s = \sum_{i=1}^{\infty} \frac{\phi_i(L_0) Q_i(s)}{M_i} M_s \begin{bmatrix} \phi_i'(L_0) k_a \\ +\phi_i(L_0) k_b \end{bmatrix} \tag{36}$$

$$k_a = \frac{k^2 D^5}{5} + \frac{2 k b_0 D^3}{4} + \frac{b_0^2 D^3}{3} \tag{37}$$

$$k_b = \frac{k^2 D^4}{4} + \frac{2 k b_0 D^3}{3} + \frac{b_0^2 D^2}{2} \tag{38}$$

$$k_c = \frac{k^2 D^3}{3} + 2 k b_0 D^2 + b_0^2 D. \tag{39}$$

In the above equations,

$$\begin{aligned} \phi_i = {} & \cosh(\lambda_i z) - \cos(\lambda_i z) \\ & - \beta_i (\sinh(\lambda_i z) - \sin(\lambda_i z)) \end{aligned} \tag{40}$$

where λ_i can be calculated by solving

$$1 + \cos(\lambda_i L) \cosh(\lambda_i L) = 0 \tag{41}$$

and

$$\beta_i = \frac{\sinh(\lambda_i L) - \sin(\lambda_i L)}{\cosh(\lambda_i L) + \cos(\lambda_i L)} \tag{42}$$

$$Q_i(s) = \frac{1}{s^2 + 2\xi_i \omega_i s + \omega^2} \tag{43}$$

in which

$$\omega_i = \frac{C_i^2}{L^2} \sqrt{\frac{YI}{\mu_v(\omega_i)}} \tag{44}$$

$$\xi_i = \frac{C_v(\omega_i)}{2\mu_v(\omega_i)\omega_i} \tag{45}$$

$$M_i(s) = \mu_v L \tag{46}$$

and

$$\begin{aligned} H_{fi}(s) = {} & \begin{pmatrix} (a-b)(a_L + b_L - c_L - d_L) \\ -\beta_i (a-b)(a_L - b_L + j c_L - j d_L) \end{pmatrix} \\ & + \frac{\alpha_0 W K \kappa_e (\gamma(s) - \tanh(\gamma(s)))}{M_i (s\gamma(s) + K \tanh(\gamma(s)))} \\ & \cdot \frac{\phi_i'(L)}{(1 + r_2 \theta(s)) \cosh(cL)} \end{aligned} \tag{47}$$

where

$$a = \frac{\alpha_0 WK\kappa_e(\gamma(s) - \tanh(\gamma(s)))}{M_i(s\gamma(s) + K\tanh(\gamma(s)))}\frac{B_s}{1 + r_2\theta(s)} \tag{48}$$

$$b = a\tanh\left(\sqrt{B(s)L}\right) \tag{49}$$

$$c = \sqrt{B(s)} \tag{50}$$

$$a_L = \frac{\sinh((c + \lambda_i)L)}{c + \lambda_i} \tag{51}$$

$$b_L = \frac{\sinh((c - \lambda_i)L)}{c - \lambda_i} \tag{52}$$

$$c_L = \frac{\sinh((c + j\lambda_i)L)}{c + j\lambda_i} \tag{53}$$

$$d_L = \frac{\sinh((c - j\lambda_i)L)}{c - j\lambda_i} \tag{54}$$

$$\theta(s) = \frac{W\kappa_e s\gamma(s)(s + K)}{h(s\gamma(s) + K)} \tag{55}$$

$$B(s) = \sqrt{r_1\left(\frac{\theta(s)}{1 + r_2\theta(s)} + \frac{2}{R_p}\right)} \tag{56}$$

$$\gamma(s) = \sqrt{\frac{s + K}{d}} \tag{57}$$

$$K = \frac{F^2 dC^-}{\kappa_e RT}(1 - C^-\Delta V) \tag{58}$$

where α_0 is an electromechanical coupling constant, d is the ionic diffusivity, R is the gas constant, F is Faraday's constant, T is the absolute temperature, C^- is the anion concentration, ΔV is the volumetric change, x is the coordinate defined in the thickness direction, κ_e is the effective dielectric constant of the polymer, r_1 is the electrode resistance per unit length in the length direction, r_2 is the electrode resistance per unit length in the thickness direction, R_p is the through-polymer resistance per unit length, and W, L, and h are the width, length, and half thickness of the IPMC beam, respectively.

4 Fabrication of robotic fish

Based on the bio-inspired design described in Sect. 2, a robotic fish was created using the following four steps: (1) fabrication of IPMC artificial fins, (2) construction of the fish body, (3) realization of the on-board circuit, and (4) assembly of the robotic fish.

4.1 Fabrication of IPMC artificial fins

The first step in creating an artificial fin is to fabricate an IPMC artificial muscle. This is based on the process developed by Chen et al. (2011). The material supplies used in the process were the following: (1) Nafion ion exchange membrane (Nafion 1110, 240 μm thick, DuPont); (2) tetraammineplatinum chloride 98% (Sigma Aldrich); (3) sodium borohydride reducing agent for reduction ($NaBH_4$, Sigma Aldrich); (4) dilute ammonium hydroxide solution (NH_4OH 29% solution, Sigma Aldrich); and (5) deionized (DI) water. The following steps were used to fabricate the IPMC:

- Step 1: Clean the Nafion film with hydrochloride acid (HCl): Boil the Nafion film in 1.0 N HCl at 80 °C for 30 min. Then rinse with DI water to remove acid residue (this step is used to remove metal particles and other impurities from the film).
- Step 2: Activate the ion exchange: In a separate beaker, mix 50 mL DI with 50 mg tetraammineplatinum chloride hydrate. Immerse the membrane in the platinum solution. Add 1 mL ammonium hydroxide 29% to balance the acid. Wait for at least 3 h.
- Step 3: Perform platinum reduction: Fill a large beaker about one-third way with DI, and add the membrane from Step 2. Heat the water to 80 °C. Mix 0.5 g sodium borohydride and 25 mL cold DI in a beaker. Add 2 mL (one full pipet) of the solution into the water bath (avoid deformation of the membrane by pouring a small amount of solution at a time). Observe the reaction of the platinum particles (a black layer of fine platinum particles should deposit on the surface of the membrane).
- Step 4: Carry out further deposition: Repeat Steps 2 and 3 to deposit more platinum on the membrane surface.

After the IPMC was fabricated, it was cut into rectangular shapes and bonded with a passive plastic film using epoxy. The fabricated caudal and pectoral fins are shown in Fig. 9.

4.2 Fish body fabrication

The fish body was used to house an on-board circuit, battery, sensors, and camera. The body needs to have a hydrodynamic shape so that drag force can be minimized. The body, designed using Autodesk Inventor, consisted of two shells clamped together using screws. Inside the shells were two chambers: one used to house the electronic circuit and battery, and the other used to provide a platform for some specific underwater applications, since this was the goal of the research. The fish body was printed with acrylonitrile butadiene styrene (ABS) material using a 3D printer (Dimension, bst1200es). Since the density of the material is lighter than water, it was easy to make the robotic fish move near the water's surface in order to receive the command from the Wi-Fi network. The fish body consisted of two chambers: the front chamber housed

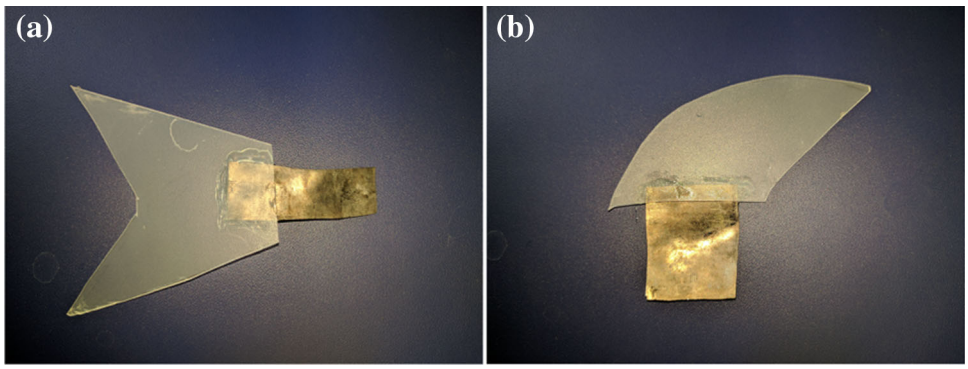

Fig. 9 Fabricated fins actuated by IPMC: **a** caudal fin; **b** pectoral fin

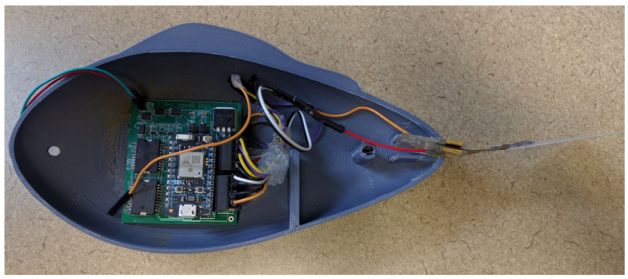

Fig. 10 Inside view of fish body

the on-board control circuit, communication device, and battery; and the rear chamber was reserved for future sensors or a camera, which could be embedded into the robotic fish for future sensing network applications. Two copper electrodes were placed at the rear, in order to provide actuation voltage signals for the pectoral fins, and one copper electrode was placed at the rear of the fish for applying a voltage signal to the caudal fin. Figure 10 shows an inside view of the fish body.

4.3 On-board circuit

A microcontroller board (Particle Photon) was used to generate three square wave control signals and communicate with a PC station through a WiFi network. Since the robotic fish swam on the surface of water, the Wi-Fi signals were receivable by placing the Wi-Fi antenna on top of the fish body and above the surface of the water. Signals S1 and S2, as shown previously in Fig. 5, were generated to drive the left and right pectoral fins, respectively. Signal S3 was generated to drive the caudal fin. Because the microcontroller draws only 25 mA and the output current goes through the IPMC up to 500 mA, three H-bridge drivers were used to provide up to 2 A peak current output to the IPMCs. The total weight of the on-board circuit plus one battery was around 20 g. The on-board circuit design is illustrated Fig. 11. A lithium ion polymer battery (Tenergy, 7.4 V, 6000 mAh) was used to provide electricity to the robotic fish.

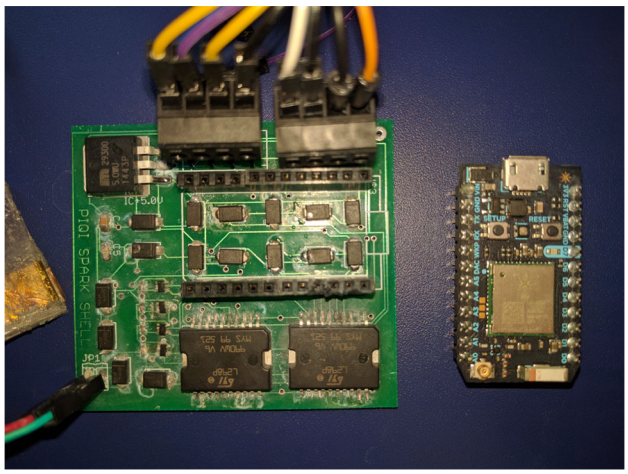

Fig. 11 On-board circuit design with particle photon

4.4 Assembled robotic fish

Figure 12 shows the assembled robotic fish. The battery and on-board circuit were put into a disposable glove (Ansell, 92-675), and the glove was sealed using tightened stainless steel wires. This water-proof treatment was adequate enough because the robot only swam on the water's surface. After putting all components into the fish body, the two shells were clamped together with screws. The total weight of the robot was 290 g. Overall, the fish had slightly positive buoyancy.

5 Experimental results

5.1 Power consumption measurement

Power consumption is one of the critical issues in an autonomous underwater vehicle. One of the advantages of using IPMC artificial fins in a robotic fish design is to utilize the low power consumption of IPMC. Chen et al. characterized the power consumption of the IPMC artificial pectoral fin (Chen et al. 2011); however, this characterization only included the power consumed by the IPMC, not

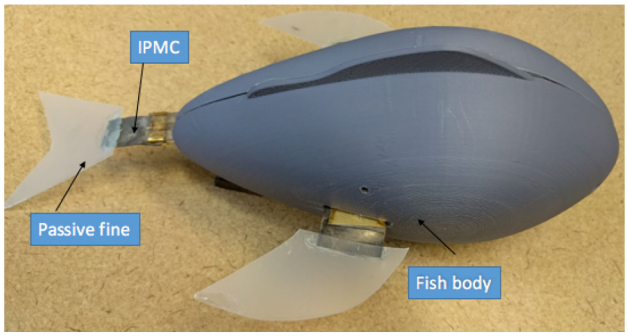

Fig. 12 Assembled robotic fish

the power consumed by the driving circuit. It was discovered that the H-Bridge became hot after a few minutes of operation. Since the energy lost in the H-Bridge is not negligible, it should be included in the total power consumption of the IPMC artificial fin. To characterize the total power consumption more accurately, an experiment was set up as follows: A DC power supply (Kepco, BOP 20-10D) was connected to the H-Bridge. Voltage was set to 7.32, 6.42, and 5.73 V. The frequency of the square wave signal, generated from the microcontroller and sent to the H-Bridge, was changed from 0.48 to 3.3 Hz. Both the output voltage and current from the DC power supply were measured. Figure 13 shows the measured voltage and current output when the actuation frequency was 0.55 Hz and the output voltage was 6.42 V. During one period, there was a peak current up to 2 A when the voltage flipped, and then the current dropped down to 500 mA.

Power consumption was calculated by

$$P = \frac{1}{T}\int_0^T i(t)u(t)dt. \tag{25}$$

where $i(t)$ is the output current, $u(t)$ is the output voltage, and T is the duration of measurement. During the test, only the caudal fin was actuated. Figure 10 shows the power consumption versus the operating frequency. Overall, the power consumption of the caudal fin was about 1 W, while the input was 7 V, and the frequency was 0.48 Hz. As shown in Fig. 14, the power consumption increased as the frequency increased. The reason why the overall power consumption was too high is that too much heat was wasted on the H-bridge. To solve this problem, in the future, it will be necessary to find a way to cool down the temperature of the H-bridge in order to improve its conversion efficiency.

5.2 Straight forward swimming test

The robotic fish was tested in a 550-gallon water tank (97 in. long, 38 in. wide, and 37 in. deep). A digital camera in an IPhone 6 smart phone was used to capture a movie of the

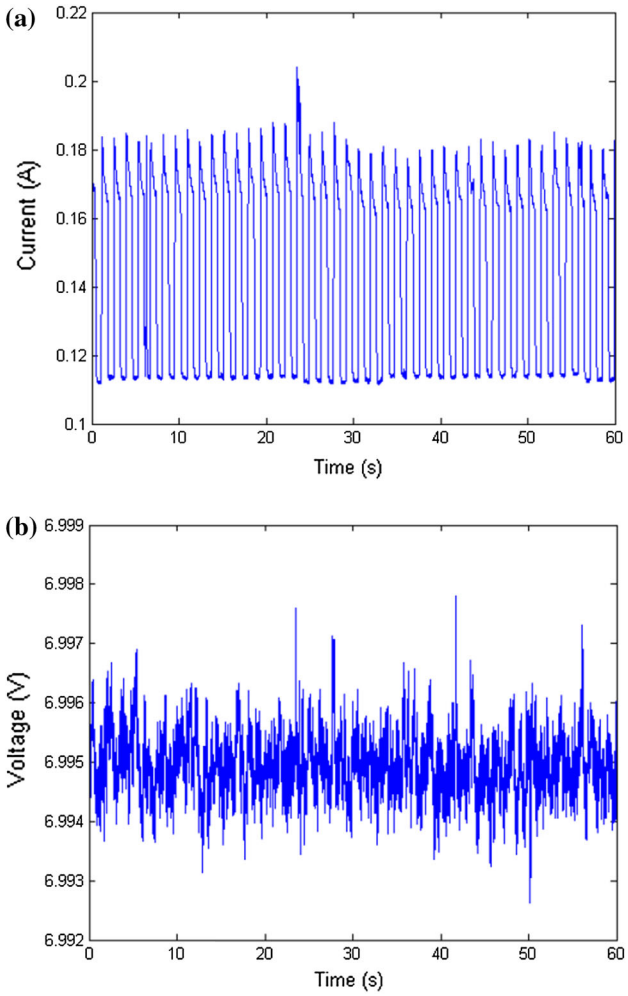

Fig. 13 Measured actuation: **a** current; **b** voltage

swimming robotic fish. Since the robotic fish's moving speed was low, the capturing instrument won't affect the result much as long as it was properly mounted. During the test, the camera was mounted on the top of the water tank. All the capturing work was done when the fish reached at steady state speed and the corresponding time information was recorded as well. Figure 15 shows six snapshots of a forward swimming test. Each snapshot was extracted every 5 s from a recorded video. The fish's forward swimming speed was controlled by changing the flapping frequency of the caudal fin. A square wave signal with 7.3 V magnitude and 0.55 Hz frequency was applied to the caudal fin. The pectoral fins were also actuated.

The swimming speed was calculated based on how long the robotic fish passed through two fixed lines. The forward swimming speed reached about 12 mm/s. Also, there was a threshold whereby the frequency was neither too high nor too low for the fish to swim. The forward speed versus the actuation frequency is shown in Fig. 16. To improve the speed, optimization of the fins and body will be necessary, which will be the focus of a future endeavor.

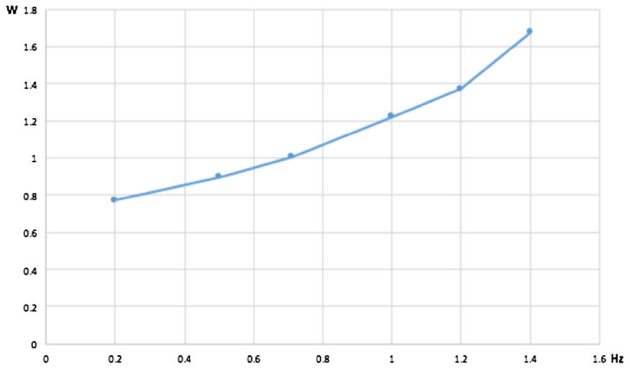

Fig. 14 Power consumption versus operating frequency and voltage

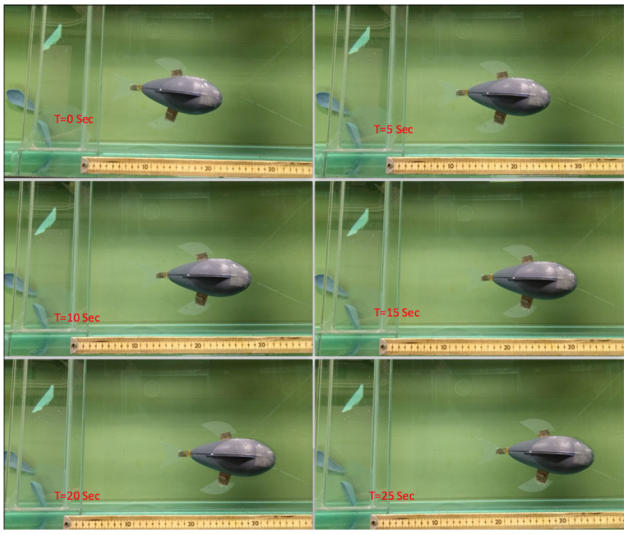

Fig. 15 Snapshots of forward-swimming test

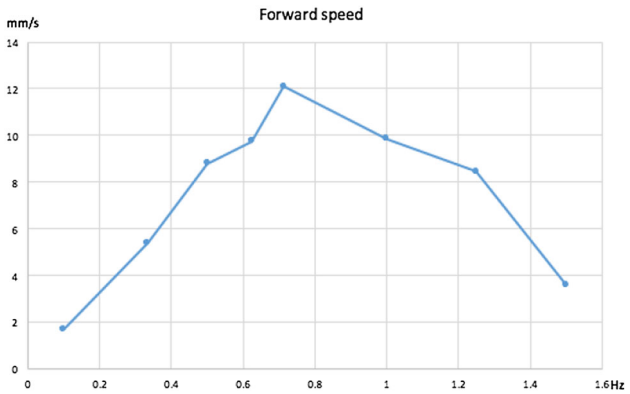

Fig. 16 Forward speed versus actuation frequency

5.3 Turning tests

Turning tests were conducted to verify the steering capability of the pectoral fin. To make a left turn, the left pectoral fin was actuated with the same actuation signal applied to the caudal fin, while the right pectoral fin was kept inactive. The caudal fin provided the forward swimming direction, while the force generated by the left pectoral fin made the fish tail turn to the left. To make a right turn, the right pectoral fin was actuated with the same actuation signal applied to the caudal fin while the left pectoral fin was kept inactive. Actuation of the right pectoral fin made the fish turn to the right (Fig. 17).

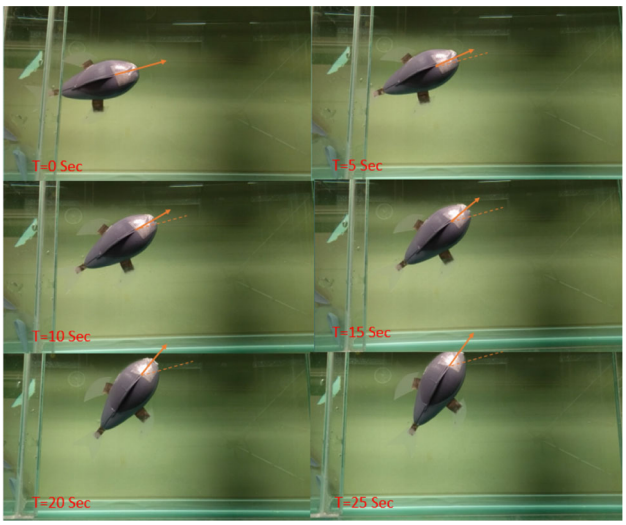

Fig. 17 Snapshots of left-turning swimming test

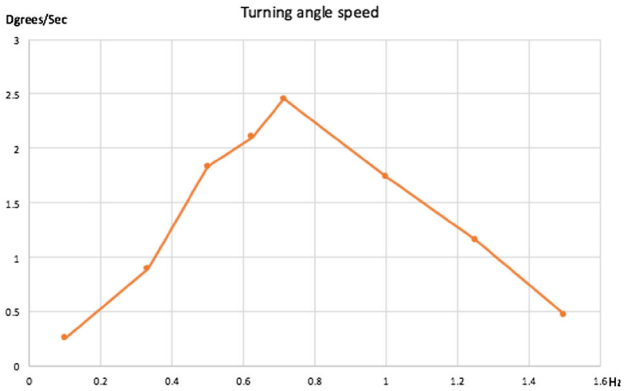

Fig. 18 Left turning speed versus actuation frequency

The left-turning speed reached about 2.5 deg/s. The right-turning speed was achieved at 2.5 deg/s. Figure 18 shows the left-turning speed versus the actuation frequency. Similar to the forward-swimming test, there were two thresholds for the actuation frequency. When the frequency was neither too high nor too low, the fish did not turn, as shown in Fig. 18. The left and right fins were not precisely same but very similar to each other. The turning speed of left and right directions were close to each other with same actuation frequency. Compared to other IMPC based robotic fish (Guo et al. 2003; Chen et al. 2010), the

Table 1 Speed of robotic fish

Frequency (Hz)	0.1	0.333	0.5	0.625	0.714	1	1.25	1.5
Forward speed (mm/s)	1.7	5.4	8.8	9.75	12.1	9.85	8.45	3.6
Left-turning speed (deg/s)	0.25	0.89	1.83	2.1	2.45	1.74	1.16	0.47

Table 2 Dimensions of caudal fin

W	B_0	B_1	L	L_0
0.015 m	0.02 m	0.04 m	0.027 m	0.018 m

Table 3 Dimensions of pectoral fin

W	B_0	B_1	S_c	L	L_0
0.02 m	0.02 m	0 m	0.04 m	0.023 m	0.018 m
x_1		x_2		θ	$\varnothing$
0.125 m		0.055 m		75.3°	24.4°

Table 4 Parameters of IPMC materials

C_v	μ_v	H	C_1
3.17	0.2 kg/m	115 μm	1.8751
Y	Γ_1	F	T
2.91×10^8 Pa	1.07 + 0.04j	96487 C/mol	300 K
R	C^-	r_1	r_2
8.3143 J/mol·K	1091 mol/m^3	210 Ω/m	0.04 Ω·m
d	K_e	R_p	α_0
5.39×10^{-9} m/s	2.48×10^{-5} F/m	38 Ω·m	0.08 J/C

forward speed is a little slower than others since this robotic fish has relatively large body size and. But it is first time to shown turning speed (maneuverability) of IPMC based robotic fish (Table 1).

6 System identification

The framework of the fish model was discussed in the previous section; here, the values needed for a valid model are measured and extracted from the experiments. The definition of the parameters shown here can be found in Sect. 3. First, the fish's body data, fin shapes, and fin locations were measured from the assembled robotic fish. The fish was 18 cm long and 8 cm wide. Table 2 shows the caudal fin's dimensions.

Then the pectoral fin was measured. The size and location information of the pectoral fin is shown in Table 3.

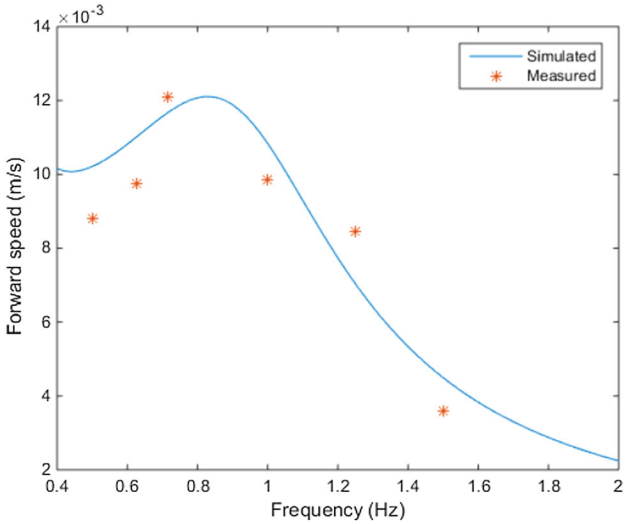

Fig. 19 Fitting result of forward speed

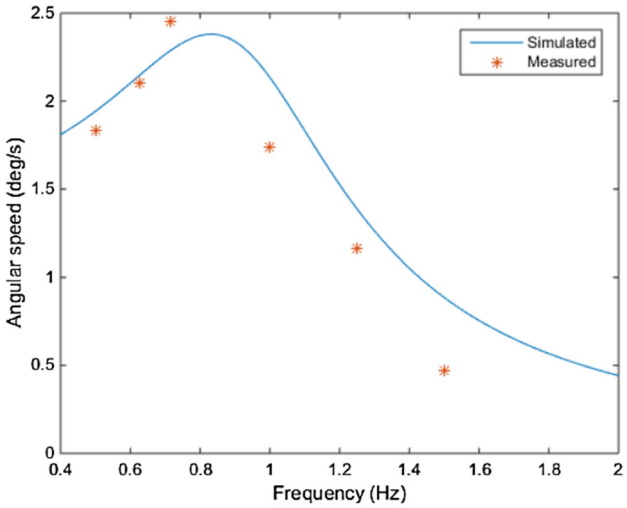

Fig. 20 Fitting result of left-turning speed

The left pectoral fin has the same parameters as the right pectoral fin because it was symmetrically installed on the fish body. The only difference is the θ angle, which is $-75.3°$ for the left pectoral fin.

Parameters of IPMC materials needed for the model calculation are shown in Table 4.

Drag coefficient C_D and drag moment coefficient C_M were extracted by fitting the model's simulation results with the experimental data. In the first step, all three fins were activated. Since the data measured with very low input frequencies were not reliable, only the speed values

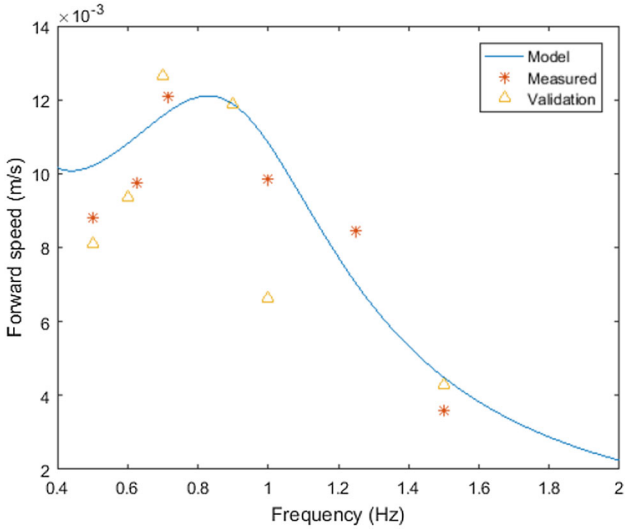

Fig. 21 Validation result of forward speed

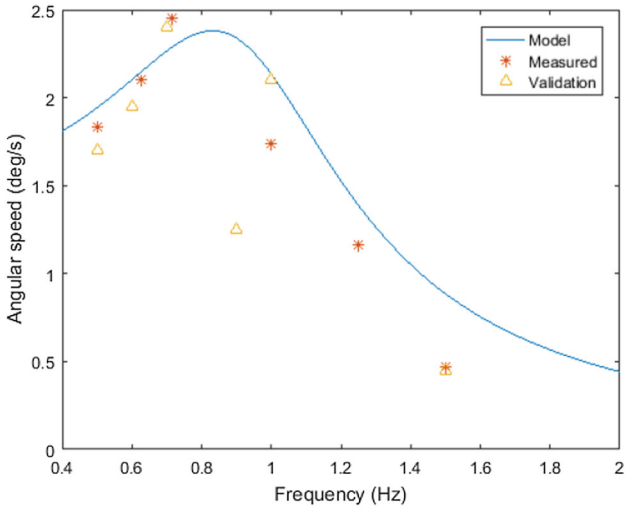

Fig. 22 Validation result of left-turning speed

with input frequency higher than 0.5 Hz were chosen. The drag coefficient C_D is finally adjusted as 425, and the fitting result of the forward speed is shown in Fig. 19.

In the next step, only one pectoral fin and caudal fin were enabled, in order to make the turning speed agree with the experimental result. The drag moment coefficient C_M was determined to be 18.5. Figure 20 shows the fitting result of the left turning speed.

Both identified C_M and C_D are in a reasonable range, compared to the reported values in (Wang and Tan 2013). Another set of experiments were performed for validation purpose. The robotic fish was using the same hardware configuration as former experiments. In these experiments, the fish's driving signals had same magnitude but different frequencies. The fish's forward speeds and turning speeds responses are put in the former figures for comparison purpose. Figures 21 and 22 show the validation results. Measurement error still existed in the new data collection, but the validation data remained near the model speed values.

7 Conclusion

This paper explains the development of a 2D maneuverable robotic fish propelled by multiple IPMC artificial fins. The robot design was inspired by a biological fish, which uses a caudal fin for its main propulsion and two pectoral fins for steering. By controlling the pectoral fins with Particle Photon, a wireless communications module, the robotic fish was able to make left and right turns as well as swim forward. This paper also derived a dynamic model for the designed robotic fish. Simulation results show that the dynamic model is capable of predicting robotic fish movement based on the dynamic model. The free-swimming tests showed that the fish can reach a forward speed of up to 12 mm/s. The left-turning and right-turning speeds can reach up to 2.5 deg/s. With the multiple-fin propulsion, the robot demonstrated its 2D maneuvering capability, which shows its potential in underwater sensing network applications.

Future research will be conducted in the following areas: (1) optimization of fish fins and fish body, (2) gait study on steering and swimming forward, (3) study on the difference between vertical motion and horizontal motion on the caudal fin, (4) motion tracking control of the robotic fish, and (5) applications in an aquatic animal behavior study.

Acknowledgements This research was supported in part by the National Science Foundation under grant CNS #1446557 and Wichita State University under the University Research/Creative Projects Award (URCA).

References

Aureli, M., Kopman, V., Porfiri, M.: Free-locomotion of underwater vehicles actuated by ionic polymer metal composites. IEEE/ASME Trans. Mechatron. **15**, 603–614 (2010)

Barbera, G.: Analisi teorica e sperimentale di un sistema di controllo per un veicolo biomimetico boxfish. Universita Degli Studi Di Padova, Padua (2009)

Bar-Cohen, Y.: Electroactive polymers as artificial muscles-capabilities, potentials and challenges. Handb. Biomim. **8**, 188–196 (2000)

Bartolini, T., Mwaffo, V., Showler, A., Macrì, S., Butail, S., Porfiri, M.: Zebrafish response to 3D printed shoals of conspecifics: the effect of body size. Bioinspir. Biomim. **11**, 026003 (2016)

Behbahani, S.B., Wang, J., Tan, X.: A dynamic model for robotic fish with flexible pectoral fins. IEEE/ASME Int. Conf. Adv. Intell. Mechatron. **2013**, 1552–1557 (2013)

Carpi, F., De Rossi, D., Kornbluh, R., Pelrine, R.E., Sommer-Larsen, P.: Dielectric elastomers as electromechanical transducers: fundamentals, materials, devices, models and applications of an emerging electroactive polymer technology. Elsevier, Amsterdam (2011)

Chen, Z., Tan, X.: A control-oriented and physics-based model for ionic polymer–metal composite actuators. IEEE/ASME Trans. Mechatron. **13**, 519–529 (2008)

Chen, Z., Hedgepeth, D.R., Tan, X.: A nonlinear, control-oriented model for ionic polymer–metal composite actuators. Smart Mater. Struct. **18**, 055008 (2009)

Chen, Z., Shatara, S., Tan, X.: Modeling of biomimetic robotic fish propelled by an ionic polymer–metal composite caudal fin. IEEE/ASME Trans. Mechatron. **15**, 448–459 (2010)

Chen, Z., Um, T.I., Bart-Smith, H.: A novel fabrication of ionic polymer–metal composite membrane actuator capable of 3-dimensional kinematic motions. Sens. Actuators **168**, 131–139 (2011a)

Chen, Z., Um, T.I., Zhu, J., Bart-Smith, H.: Bio-inspired robotic cownose ray propelled by electroactive polymer pectoral fin. ASME 2011 Int. Mech. Eng. Congr. Expo. **26**, 817–824 (2011b)

Chen, Z., Um, T.I., Bart-Smith, H.: Bio-inspired robotic manta ray powered by ionic polymer–metal composite artificial muscles. Int. J. Smart Nano Mater. **3**, 296–308 (2012)

Evologics: Subsea glider with fin ray effect. https://www.evologics.de/en/products/glider/index.html (2009). Accessed 1 Feb 2017

Festo: Aqua ray inspired by the manta ray. https://www.festo.com/group/en/cms/10246.htm (2008). Accessed 1 Feb 2017

Gao, J., Bi, S., Xu, Y., Liu, C.: Development and design of a robotic manta ray featuring flexible pectoral fins. IEEE Int. Conf. Robot. Biomim. ROBIO **2007**, 519–523 (2007)

Guo, J.: A waypoint-tracking controller for a biomimetic autonomous underwater vehicle. Ocean Eng. **33**, 2369–2380 (2006)

Guo, S., Fukuda, T., Asaka, K.: A new type of fish-like underwater microrobot. IEEE/ASME Trans. Mechatron. **8**, 136–141 (2003)

Hu, W.-R.: Hydrodynamic study on a pectoral fin rowing model of a fish. J. Hydrodyn. Ser. B **21**, 463–472 (2009)

Hu, H., Liu, J., Dukes, I., Francis, G.: Design of 3D swim patterns for autonomous robotic fish. IEEE/RSJ Int. Conf. Intell. Robots Syst. **2006**, 2406–2411 (2006)

Kim, B., Kim, D.-H., Jung, J., Park, J.-O.: A biomimetic undulatory tadpole robot using ionic polymer–metal composite actuators. Smart Mater. Struct. **14**, 1579 (2005)

Kodati, P., Hinkle, J., Deng, X.: Micro autonomous robotic ostraciiform (MARCO): design and fabrication. IEEE Int. Conf. Robot. Autom. **2007**, 960–965 (2007)

Kopman, V., Laut, J., Acquaviva, F., Rizzo, A., Porfiri, M.: Dynamic modeling of a robotic fish propelled by a compliant tail. IEEE J. Ocean. Eng. **40**, 209–221 (2015)

Lauder, G.V., Anderson, E.J., Tangorra, J., Madden, P.G.: Fish biorobotics: kinematics and hydrodynamics of self-propulsion. J. Exp. Biol. **210**, 2767–2780 (2007)

Lauder, G., Madden, P., Tangorra, J., Anderson, E., Baker, T.: Bioinspiration from fish for smart material design and function. Smart Mater. Struct. **20**, 094014 (2011)

Lighthill, M.: Aquatic animal propulsion of high hydromechanical efficiency. J. Fluid Mech. **44**, 265–301 (1970)

Morgansen, K.A., Triplett, B.I., Klein, D.J.: Geometric methods for modeling and control of free-swimming fin-actuated underwater vehicles. IEEE Trans. Robot. **23**, 1184–1199 (2007)

Mwaffo, V., Butail, S., Porfiri, M.: In-silico experiments of zebrafish behaviour: modeling swimming in three dimensions. Sci. Rep. **7**, 39877 (2017)

Najem, J., Sarles, S.A., Akle, B., Leo, D.J.: Biomimetic jellyfish-inspired underwater vehicle actuated by ionic polymer metal composite actuators. Smart Mater. Struct. **21**, 094026 (2012)

Pelrine, R., Kornbluh, R., Pei, Q., Joseph, J.: High-speed electrically actuated elastomers with strain greater than 100%. Science **287**, 836–839 (2000)

Punning, A., Anton, M., Kruusmaa, M., Aabloo, A.: A biologically inspired ray-like underwater robot with electroactive polymer pectoral fins. Int. IEEE Conf. Mechatron. Robot. **2004**, 241–245 (2004)

Ruberto, T., Mwaffo, V., Singh, S., Neri, D., Porfiri, M.: Zebrafish response to a robotic replica in three dimensions. R. Soc. Open Sci. **3**, 160505 (2016)

Ryuh, Y.-S., Yang, G.-H., Liu, J., Hu, H.: A school of robotic fish for mariculture monitoring in the sea coast. J. Bionic Eng. **12**, 37–46 (2015)

Shahinpoor, M., Kim, K.J.: Ionic polymer-metal composites: I. Fundamentals. Smart Mater. Struct. **10**, 819 (2001)

Shao, J., Wang, L., Yu, J.: Development of an artificial fish-like robot and its application in cooperative transportation. Contr. Eng. Pract. **16**, 569–584 (2008)

Suo, Z.: Theory of dielectric elastomers. Acta Mech. Solida Sin. **23**, 549–578 (2010)

Tan, X., Kim, D., Usher, N., Laboy, D., Jackson, J., Kapetanovic, A., et al.: An autonomous robotic fish for mobile sensing. IEEE/RSJ Int. Conf. Intell. Robots Syst. **2006**, 5424–5429 (2006)

Villanueva, A., Smith, C., Priya, S.: A biomimetic robotic jellyfish (Robojelly) actuated by shape memory alloy composite actuators. Bioinspir. Biomim. **6**, 036004 (2011)

Walker, J.A.: Dynamics of pectoral fin rowing in a fish with an extreme rowing stroke: the threespine stickleback (*Gasterosteus aculeatus*). J. Exp. Biol. **207**, 1925–1939 (2004)

Wang, J., McKinley, P. K., Tan, X.: Dynamic modeling of robotic fish with a flexible caudal fin. In: Proceeding ASME 2012 5th Annual Dynamic Systems and Control Conference joint with the JSME 2012 11th Motion and Vibration Conference, pp. 203–212 (2012)

Wang, J., Tan, X.: A dynamic model for tail-actuated robotic fish with drag coefficient adaptation. Mechatronics **23**, 659–668 (2013)

Wang, Y., Tan, R., Xing, G., Wang, J., Tan, X., Liu, X., et al.: Aquatic debris monitoring using smartphone-based robotic sensors. In: Proceedings of the 13th international symposium on Information processing in sensor networks. pp. 13–24 (2014)

Wang, Z., Wang, Y., Li, J., Hang, G.: A micro biomimetic manta ray robot fish actuated by SMA. IEEE Int. Conf. Robot. Biomim **2009**, 1809–1813 (2009)

Wang, J., McKinley, P.K., Tan, X.: Dynamic modeling of robotic fish with a base-actuated flexible tail. J. Dyn. Syst. Meas. Contr. **137**, 011004 (2015)

y Alvarado, P.V., Youcef-Toumi, K.: Design of machines with compliant bodies for biomimetic locomotion in liquid environments. J. Dyn. Syst. Meas. Control **128**, 3–13 (2006)

Ye, X., Su, Y., Guo, S.: A centimeter-scale autonomous robotic fish actuated by IPMC actuator. IEEE Int. Conf. Robot. Biomim. **2007**, 262–267 (2007)

Yeom, S.-W., Oh, I.-K.: A biomimetic jellyfish robot based on ionic polymer metal composite actuators. Smart Mater. Struct. **18**, 085002 (2009)

Yu, J., Tan, M., Wang, S., Chen, E.: Development of a biomimetic robotic fish and its control algorithm. IEEE Trans. Syst. Man Cybern. **34**, 1798–1810 (2004)

Zhou, C., Low, K.: Design and locomotion control of a biomimetic underwater vehicle with fin propulsion. IEEE/ASME Trans. Mechatron. **17**, 25–35 (2012)

Zienkiewicz, A., Barton, D., Porfiri, M., Di Bernardo, M.: Leadership emergence in a data-driven model of zebrafish shoals with speed modulation. Eur. Phys. J. Spec. Top. **224**, 3343–3360 (2015)

Mr. Zhihang Ye was born in China. He received his Bachelor's Degree in Electrical Engineering from Shandong University in China in 2008, and his Master's Degree in Control Science and Engineering from Tongji University in China in 2012. Since August 2013, Mr. Ye has been pursuing his PhD degree in Electrical Engineering at Wichita State University. His research interests are focused on smart materials, control systems, and bio-inspired robotics. Mr. Ye received the Maggie Sawan Fellowship in 2014.

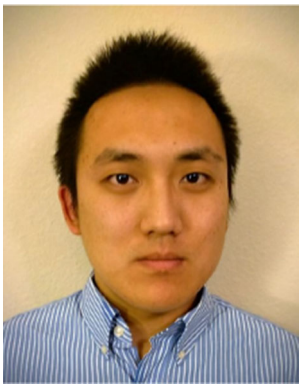

Mr. Piqi Hou received his B.S. degree in Electrical Engineering from Wichita State University in 2014 and his M.S. Degree in Electrical and Computer Engineering at Wichita State University in 2016. His current research interests include the modeling and control of electrical-active polymers and the development of highly maneuverable bio-inspired robotic fish.

Dr. Zheng Chen is an assistant professor in the Department of Electrical Engineering and Computer Science at Wichita State University (WSU). He received his B.E. degree in Electrical Engineering and his M.E. degree in Control Science & Engineering from Zhejiang University, China, in 1999 and 2002, respectively. He received his PhD degree in Electrical Engineering from Michigan State University (MSU) in 2009. Dr. Chen joined the Department of Mechanical & Aerospace Engineering at the University of Virginia as a research associate in Sept. 2009. Dr. Chen joined Baker Hughes as a research and development engineer specializing in control systems in July 2012. Since August 2013, Dr. Chen has been with WSU. His research interests include dynamic systems and control, smart material sensors and actuators, and bio-inspired underwater robots. Dr. Chen received a First Award from Kansas NSF EPSCoR and an NSF CAREER Award in 2016.